2014 IEEE International Conference on Robotics & Automation (ICRA)
Hong Kong Convention and Exhibition Center
May 31 - June 7, 2014. Hong Kong, China

Design of a force-decoupled compound parallel alignment stage for high-resolution imprint lithography

Xiantao Sun[1], Weihai Chen[1], Rui Zhou[1], Wenjie Chen[2], and Jianbin Zhang[3]

Abstract— **Parallel surface contact between the template and the substrate is very important in imprint lithography. In this paper, a novel force-decoupled compound parallel alignment stage is proposed for high-resolution imprint lithography. It mainly consists of a high-stiffness spherical air bearing (SAB) and a multi-degree-of-freedom (multi-DOF) flexure-based mechanism that functions for both the active and passive alignments. Apart from the function of the parallel alignment, the proposed stage can also endure a large imprinting force of more than 1000 N but does not cause any damage to the delicate components, which is mainly attributed to its force-decoupled characteristic. Through the stiffness modeling and finite element analysis (FEA), the performance is evaluated to satisfy the design requirement. Finally, experimental tests are conducted on the parallel alignment stage for the hot embossing process, and the grating patterns with linewidth of 2.5 μm are successfully transferred from the silicon template to the polymethy methacrylate (PMMA) substrate. This result demonstrates that the proposed stage can be used in the hot embossing process without degrading its alignment accuracy.**

I. Introduction

Nanoimprint lithography (NIL) is a new method to fabricate micro/nano patterns due to its simplicity, high replication fidelity, low cost and high throughput, etc, and it is usually considered as a promising technique for the next generation lithography (NGL) [1], [2]. Unlike the conventional photolithography and other NGL techniques, NIL mainly relies on the physical deformation of the resist and has been successfully utilized in the fabrication of micro/nano structures [3]-[6]. The resolution of NIL is mainly determined by the minimum feature size on the template that can be fabricated, thus it can achieve a very high resolution within a few nanometers. Moreover, the parallel surface contact between the template and the substrate is very important for pattern fidelity in NIL, whereas the nonparallel surface contact will lead to the uneven patterns on the substrate [7]-[9]. In this light, the parallel alignment stage is usually utilized to compensate for this parallel error.

For the parallel alignment stages, research attentions have been focused on three categories, namely, the passive, active and compound alignment stages, which usually resort to the flexure-based mechanism due to the merits of no backlash, no friction, and free lubrication [10]-[14]. The passive alignment stage is to utilize the elastic deformation of flexible elements to passively eliminate the parallel error between the template and the substrate, whereas the active one is to utilize the high-resolution sensors for error detection and then to actively eliminate it. It is conceivable that the compound alignment stage is the combination of the above two stages. Normally, the passive alignment stage has a simpler structure, and the active one comes second, followed by the most complicated compound one. Lee *et al*. developed a six-DOF passive compliant stage for the complete surface contact between the template and the substrate [15], [16]. It consisted of an inner mechanism and an outer mechanism connected in series for the in-plane and out-of-plane motions, respectively. Jia *et al*. described a three-DOF actively controlled compliant parallel stage utilizing flexure hinges for NIL [17]. The stiffness of the overall system was analyzed using the matrix method. Choi *et al*. designed a compound parallel alignment stage for step and flash imprint lithography [18]. The orientation of the template with respect to the substrate was first manually adjusted by using three differential micrometers, and then a two-DOF passive rotational flexure-based stage was utilized to eliminate the residual parallel error.

Unfortunately, the existing techniques used in the design of NIL alignment systems do not consider the issue of delicate components within the imprinting force transmission loop, thus resulting in a problem that the alignment accuracy cannot be guaranteed especially under a large imprinting force. To address this problem, this paper will comprehensively analyze and study the fundamental working principle of NIL machine and proposes a novel design approach to the parallel alignment stage with the function of decoupling the large imprinting force from the delicate components. It mainly consists of a high-stiffness spherical air bearing (SAB) and a multi-DOF flexure-based mechanism. The large imprinting force is supported by the high-stiffness SAB, whereas only the small bending moment due to the nonuniform imprinting force can reach the delicate flexure-based mechanism. Thus, this approach will make the alignment system able to be used not only for the ultraviolet (UV) imprinting process, but also for the hot embossing process. Finally, the validity and feasibility of the research approach will be verified through an actual experimental prototype. We believe that this research will provide the theoretical and technical supports for the development of precision NIL machines, and meanwhile will lay a solid foundation for the research of micro/nano-fabrication consistency and mass production.

*Manuscript received September 14, 2013. This research is supported by the National Natural Science Foundation of China under Grant Nos. 91023036 and 51275018, and Research Fund for the Doctoral Program of Higher Education of China under Grant No. 20131102110010.

[1]X. Sun, W. Chen, and R. Zhou are with the School of Automation Science and Electrical Engineering, Beihang University, Beijing, 100191, China xiantaosun@163.com,(whchen,zhr)@buaa.edu.cn

[2]W. Chen is with the Singapore Institute of Manufacturing Technology, 638075, Singapore wjiechen@yahoo.com.sg

[3]J. Zhang is with the School of Mechanical Engineering and Automation, Beihang University, Beijing, 100191, China jbzhangbuaa@163.com

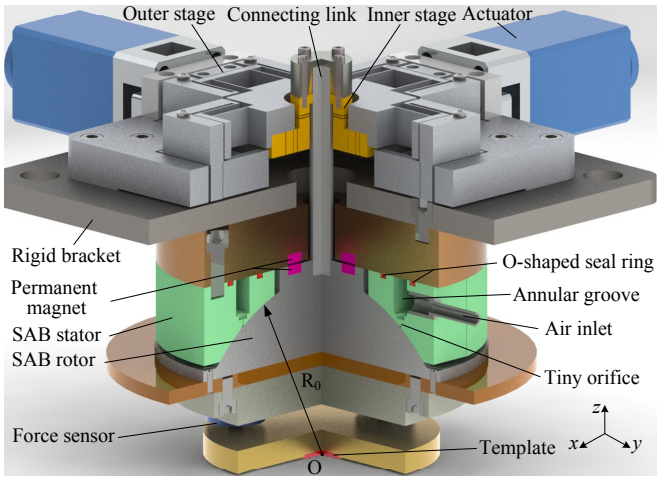

Fig. 1. Cross-sectional view of the developed force-decoupled compound parallel alignment stage

II. Mechanical Design

The force-decoupled compound parallel alignment stage for NIL is developed as shown in Fig. 1. It can be seen that the alignment stage mainly consists of a high-stiffness SAB with a bowl-shaped stator and a hemispherical rotor, a magnetic preload mechanism, and a multi-DOF flexure-based mechanism that functions for the active and passive alignments. Moreover, three uniformly distributed force sensors (not all shown in the figure) are utilized to measure the imprinting force distribution over the template.

In order to achieve a frictionless two-DOF rotation of the SAB rotor about the x- and y-axes for the parallel alignment, the pressurized air from the air inlet is transmitted to the stator-rotor interface to form a thin air film through twelve uniformly distributed tiny orifices. For a good airtight condition, two O-shaped seal rings are placed at the inner and outer sides of the annular groove, respectively. Moreover, the template center O coincides with the spherical center of the SAB stator or rotor to avoid the lateral motion of the template due to its tilt. Two sets of annular permanent magnets are mounted in the stator and the rotor, respectively, to balance the gravity of the rotor and provide a preload to the air film for maximizing its stiffness and maintaining a constant thickness [19]. The material of the stator and the rotor is magnetic stainless steel with high permeability to avoid the magnetic flux leakage.

For the multi-DOF flexure-based mechanism, it mainly consists of an outer stage and an inner stage. The outer stage is a decoupled parallel XY stage with a two-layer stacked structure. Its in-plane translations are driven by two high-precision linear actuators. The inner stage attached to the output end of the outer stage is a serial combination of a serial XY stage and a three-DOF (i.e., θ_x, θ_y and z) out-of-plane stage. Moreover, the inner stage is connected to the SAB rotor through a connecting link. It is known that the SAB can provide the three-DOF rotational motions, but only the rotational motions about the x- and y-axes are required for the parallel alignment in NIL. However, the five-DOF structure design of the inner stage can effectively restrict the undesired self-rotation (θ_z) of the SAB rotor.

As shown in Fig. 2(a), the initial parallel error θ_0 between the template and the substrate is inevitable due to the manufacturing and assembly errors. During the imprinting process, the z-axis actuator first brings the template in contact with the substrate until a small imprinting force can be detected as shown in Fig. 2(b). However, the parallel error will cause the different results of three force sensors. These force signals will be sent to the control system to further drive the outer stage through two linear actuators and then actively adjust the tilt of the template as shown in Fig. 2(c). After the active alignment, most of the parallel error can be eliminated, but there still remains a small parallel error θ' due to the limited precision of the adopted actuators and force sensors. Subsequently, assuming the contact position "A" between the template and the substrate, as the imprinting force F continues to increase, it can be transformed into a vertical force F acting on the template center and a bending moment M as shown in Fig. 2(d). The vertical force F is supported by the high-stiffness air film, whereas the bending moment M drives the inner stage to passively adjust the tilt of the template until eliminating the residual parallel error θ'. This also further realizes the function of decoupling the large imprinting force from the delicate components.

III. Analysis and Modeling for the Parallel Alignment Stage

A. Adjusting Angle Analysis

According to the pseudo-rigid-body model (PRBM) approach, the parallel XY stage (i.e., the outer stage) and the serial XY stage can be equivalent to an active prismatic joint

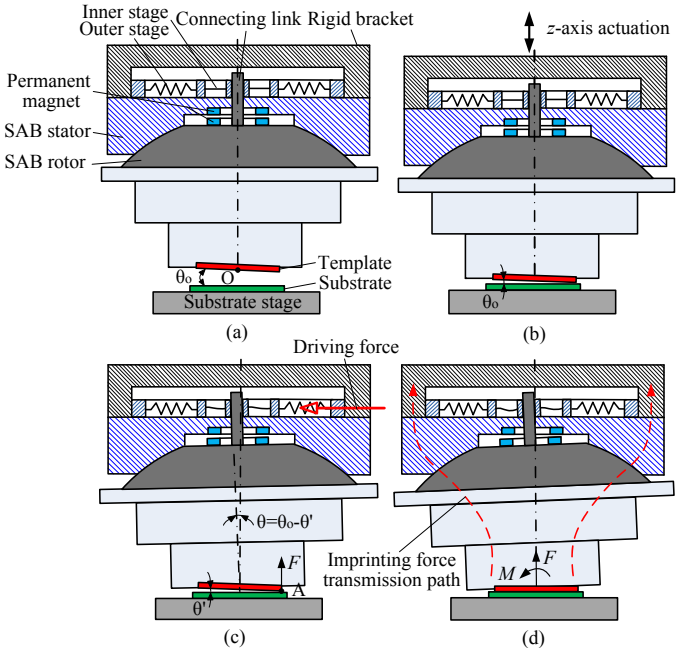

Fig. 2. (a) Schematic diagram of the parallel alignment stage, (b) z-axis actuation, (c) active alignment, and (d) passive alignment

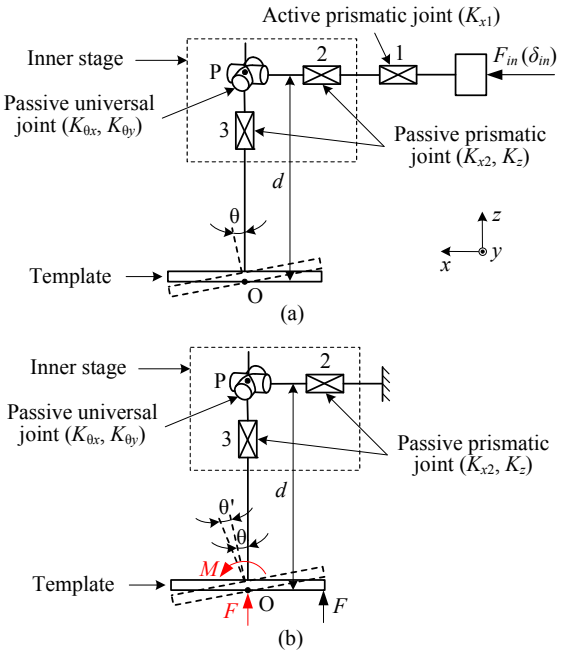

Fig. 3. Simplified model of the parallel alignment stage for (a) the active and (b) passive alignments

1 and a passive prismatic joint 2 along the x- or y-axis, respectively. Similarly, the three-DOF out-of-plane stage can be also equivalent to a passive universal joint and a passive prismatic joint 3 along the z-axis, which are connected in series, and their motion axes intersect at one point P. It is noticed that the "active" joint means that it is directly driven by the actuator and conversely it is a "passive" joint. Thus, it is obvious that only the prismatic joint 1 is the active one. Due to the symmetric structure, the parallel alignment stage has the identical performance along the x- and y-axes. Further, its simplified model along the x-axis is obtained as shown in Fig. 3, where K_i represents the stiffness of the corresponding equivalent joint.

For the active alignment as shown in Fig. 3(a), the template actively generates a tilting angle θ around its center O under the input force/displacement (F_{in}/δ_{in}) from the x-actuator. Considering the distance d of the point P deviating from the template center O, for a small tilting angle θ, its displacements along the x- and z-axes can be obtained, respectively, as follows

$$\delta_{Px} = d\sin\theta \cong d\theta \tag{1}$$

$$\delta_{Pz} = d\cdot(1-\cos\theta) \cong (1/2)\,d\theta^2 \tag{2}$$

Under the equilibrium status for the parallel XY stage, the input force can be derived as

$$F_{in} = K_{x1}\cdot\delta_{in} + K_{x2}\cdot(\delta_{in}-\delta_{Px}) \tag{3}$$

where $\delta_{in}-\delta_{Px}$ represents the relative displacement of the passive prismatic joint 2.

Moreover, during the initial surface contact between the template and the substrate, the small imprinting force as the feedback signal has a small influence on the deformation of the flexure-based components. Thus, according to the conservation of energy, the following equation is obtained as

$$\frac{1}{2}F_{in}\delta_{in} = \frac{1}{2}K_{x1}\delta_{in}^2 + \frac{1}{2}K_{x2}(\delta_{in}-\delta_{Px})^2 + \frac{1}{2}K_\theta\theta^2 + \frac{1}{2}K_z\delta_{Pz}^2 \tag{4}$$

Then, substituting (1)-(3) into (4) yields the relationship between the tilting angle of the template and the required input force as

$$F_{in} = \frac{d^2K_{x1}K_{x2}+K_{x1}K_\theta+K_{x2}K_\theta}{dK_{x2}}\cdot\theta + \frac{dK_z(K_{x1}+K_{x2})}{4K_{x2}}\cdot\theta^3 \tag{5}$$

Whereas, during the passive alignment process, the actively controlled actuators do not generate any outputs, thus the output end of the parallel XY stage is fixed as shown in Fig. 3(b). The large imprinting force F can be transformed into a vertical force F acting on the template center O and a bending moment M given by $M = (1/2)\,Fl_0$, where l_0 is the length of the template. The former almost does not cause any motions due to the high-stiffness air film, whereas the latter drives the inner stage to passively adjust the tilt of the template until eliminating the residual parallel error θ'. Similarly with (4), the work done by the bending moment is given as

$$\frac{1}{2}M\theta' = \frac{1}{2}K_{x2}\left[(\delta_{in}-d\theta+d\theta')^2-(\delta_{in}-d\theta)^2\right]$$

$$+\frac{1}{2}K_\theta\left[(\theta+\theta')^2-\theta^2\right]+\frac{1}{2}K_z\left[\frac{d^2(\theta+\theta')^4}{4}-\frac{d^2\theta^4}{4}\right] \tag{6}$$

Thus, after the active and the passive alignments, the total adjusting angle of the parallel alignment stage is

$$\theta_0 = \theta+\theta' \tag{7}$$

B. Stiffness Modeling

For the parallel XY stage, it consists of four flexure modules A for the bottom layer and four flexure modules B for the top layer. After the assembly of the bottom and top layers, it forms four parallel kinematic chains that connect the output end to the fixed base, each of which has two serially connected modules A and B. Moreover, in order to kinematically decouple the output motions along the x- and y-axes in the maximum extent, any two adjacent chains are orthogonal to each other [20], [21]. Similarly, the serial XY stage includes two flexure modules C connected in parallel in the x or y direction. It can be seen that although each module has different numbers of flexure beams, each module utilizes the secondary stage to increase the motion of the primary stage, where the former only moves half of the latter, as shown in Fig. 4.

According to the force analysis of a single flexure beam, the stiffness of the flexure modules A, B and C can be obtained, and the detailed stiffness modeling can be found in [20]. Further, the stiffness of the parallel and serial XY

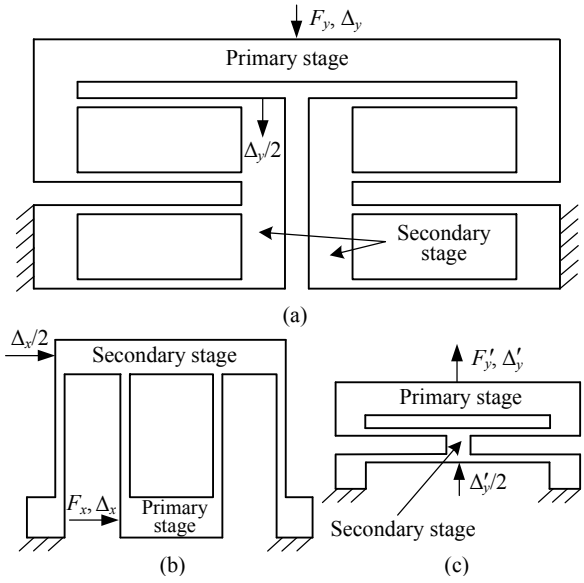

Fig. 4. Three basic flexure modules: (a) module A for the bottom layer, (b) module B for the top layer of the parallel XY stage, and (c) module C for the serial XY stage

stages can be obtained according to the parallel relationship of flexure modules, respectively, as follows

$$K_{x1} = 2K_{\mathrm{A}} + 2K_{\mathrm{B}} = \frac{4Eb_{\mathrm{A}}t_{\mathrm{A}}^3}{l_{\mathrm{A}}^3} + \frac{2Eb_{\mathrm{B}}t_{\mathrm{B}}^3}{l_{\mathrm{B}}^3} \tag{8}$$

$$K_{x2} = 2K_{\mathrm{C}} = \frac{2Eb_{\mathrm{C}}t_{\mathrm{C}}^3}{l_{\mathrm{C}}^3} \tag{9}$$

where K_i (i = A, B and C) is the stiffness of flexure module i along the motion direction, l_i, b_i and t_i are the length, width and thickness of the flexure beam, respectively, and E is the young's modulus of the material.

As shown in Fig. 1, the three-DOF out-of-plane stage is composed of a tapered split flexure clamp and an annular flexure plate. It can be seen from Fig. 5(a) that the annular flexure plate includes four portions (I, II, III and IV) that

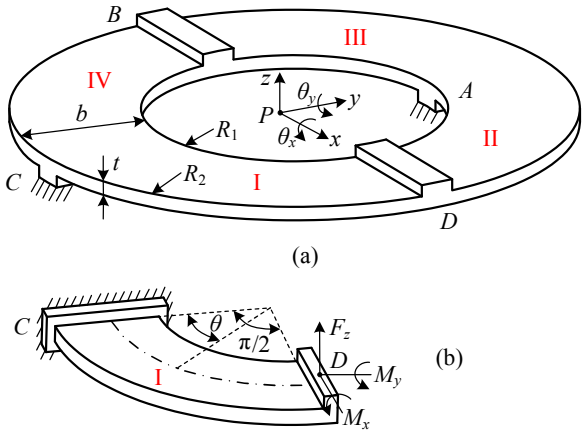

Fig. 5. Three-DOF out-of-plane stage: (a) annular flexure plate and (b) one quarter model

are separated by two fixed ends (A and C) and two free ends (B and D). Due to the symmetric structure, one quarter model is selected for the purpose of analysis, as shown in Fig. 5(b). Moreover, since the in-plane forces (F_x, F_y and M_z) have no impact on the out-of-plane motions of the annular flexure plate, only the out-of-plane forces (F_z, M_x and M_y) are considered, and the bending moment and torque for any position are given, respectively, as follows

$$M(\theta) = F_z R\cos\theta + M_x \sin\theta - M_y \cos\theta \tag{10}$$

$$T(\theta) = F_z R(1-\sin\theta) + M_x \cos\theta + M_y \sin\theta \tag{11}$$

where R is the average radius of the annular flexure plate, and satisfies $R = (R_1 + R_2)/2$, and R_1 and R_2 are the radius of the inner and outer rings, respectively.

The displacements of the point D can be obtained based on the unit-load method. The translation along the z-axis is given as

$$\begin{aligned}\delta_z &= \int_0^{\frac{\pi}{2}} \frac{M(\theta)\bar{M}(\theta)_z}{EI}\cdot Rd\theta + \int_0^{\frac{\pi}{2}} \frac{T(\theta)\bar{T}(\theta)_z}{GI_p}\cdot Rd\theta \\ &= c_{11}F_z + c_{12}M_x + c_{13}M_y\end{aligned} \tag{12}$$

where $\bar{M}(\theta)_z$ and $\bar{T}(\theta)_z$ are the corresponding unit loads and given by $\bar{M}(\theta)_z = R\cos\theta$ and $\bar{T}(\theta)_z = R(1-\sin\theta)$, respectively, $G = E/(2(1+\gamma))$ is the shear modulus of the material, and $I_p = bt^3\left[(1/3) - 0.21\,(t/b)\left(1-\left(t^4/12b^4\right)\right)\right]$ is the torsional moment of inertia of the cross section [22]. It is noted that the shoulder width of the free or fixed end is not taken into consideration for modeling simplification.

Similarly, the rotation angles about the x- and y-axes can be obtained, respectively, as follows

$$\theta_x = c_{21}F_z + c_{22}M_x + c_{23}M_y \tag{13}$$

$$\theta_y = c_{31}F_z + c_{32}M_x + c_{33}M_y \tag{14}$$

Then, according to (12)-(14), for the flexure plate I, the force-deformation relationship at the free end D can be written in the matrix form as

$$\begin{pmatrix}\delta_z\\ \theta_x\\ \theta_y\end{pmatrix} = \begin{pmatrix}c_{11} & c_{12} & c_{13}\\ c_{21} & c_{22} & c_{23}\\ c_{31} & c_{32} & c_{33}\end{pmatrix}\begin{pmatrix}F_z\\ M_x\\ M_y\end{pmatrix} = C_0\begin{pmatrix}F_z\\ M_x\\ M_y\end{pmatrix} \tag{15}$$

where C_0 is the compliance matrix of the flexure plate I, and satisfies $c_{ij} = c_{ji}$ (i, j = 1, 2, 3), and its inverse is defined as the stiffness matrix as follows

$$K_0 = C_0^{-1} = \begin{pmatrix}k_{11} & k_{12} & k_{13}\\ k_{21} & k_{22} & k_{23}\\ k_{31} & k_{32} & k_{33}\end{pmatrix} \tag{16}$$

Considering that the portions I, II, III and IV are connected in parallel, based on the matrix method [23], [24], the stiffness matrix of the entire out-of-plane stage can be derived as

$$\begin{aligned}K &= diag\begin{pmatrix}4k_{11} & 4k_{22} & 4R^2k_{11} - 4Rk_{31} - 4Rk_{13} + 4k_{33}\end{pmatrix}\\ &= diag\begin{pmatrix}K_z & K_{\theta x} & K_{\theta y}\end{pmatrix}\end{aligned} \tag{17}$$

IV. Finite Element Analysis

In order to evaluate the performance of the parallel alignment stage, the finite element analysis is performed with commercial software ANSYS 11.0. Based on the geometrical model as shown in Fig. 1, the finite element model is established and then meshed using a three-dimensional 20-node solid element named SOLID 95. This kind of solid element is very suitable to model the irregular shapes such as flexure elements. Moreover, the geometrical parameters of flexure elements are given as: l_A = 21 mm, b_A = 16 mm, t_A = 0.6 mm, l_B = 21 mm, b_B = 16 mm, t_B = 0.6 mm, l_C = 12 mm, b_C = 10 mm, t_C = 0.5 mm, R = 10 mm, b = 6 mm, and t = 0.6 mm. AL7075-T651 is selected as the material of all flexure stages due to its high strength, high elasticity and light mass. Moreover, the meshes are refined at the flexure elements with respect to the remaining parts to guarantee the simulation accuracy.

In the case of the single-axis drive, an input force F_{in} of 150 N is applied at the input end of the parallel XY stage to adjust the template orientation. The simulation result indicates that the template can generate a tilting angle of about 5.3 mrad, which meets the design requirement for the active alignment. Nevertheless, in the case of the double-axis drive, the tilting angles of the template about the x- and y-axes are 4.9 mrad and 5.1 mrad, respectively. The deviation from the single-axis drive is attributed to the coupling effect between the two drive axes. The resulting maximum stress within the flexure elements is 152.5 MPa and far less than the yield strength of the material. Moreover, the template strictly rotates about its surface center, which benefits from the coincidence between the template center and the spherical center of the SAB rotor.

V. Experimental Tests

During the imprinting experiment, the alignment accuracy of most of the existing alignment stages cannot be guaranteed especially in the hot embossing process due to the large imprinting force. Moreover, the force-decoupled characteristic of the developed alignment stage for the UV imprinting process will be not obvious due to its small imprinting force. Thus, we will only conduct the hot embossing process to validate the performance of the developed alignment stage.

The final experimental apparatus setup is shown in Fig. 6. The NIL machine is mounted on a heavy marble base with a thin rubber cushion attached to its bottom to reduce the external vibration disturbances on the pattern transfer between the template and the substrate. A z-axis actuator and a preloaded ball screw are employed to realize the vertical imprint motion, where four precision cylinders are to guide this motion. Two actuators in the xy plane are utilized to implement the active alignment between the template and the substrate. The substrate temperature can be accurately controlled by the thermal control unit that consists of several cartridge heaters and thermocouples embedded within the substrate stage. Aluminum alloy is selected as the material of the substrate stage to achieve the high thermal conductivity. Three high-precision force sensors are utilized to measure the imprinting force distribution over the template for the closed-loop feedback during the active alignment. Moreover, an air compressor is required to provide the pressurized air for the SAB.

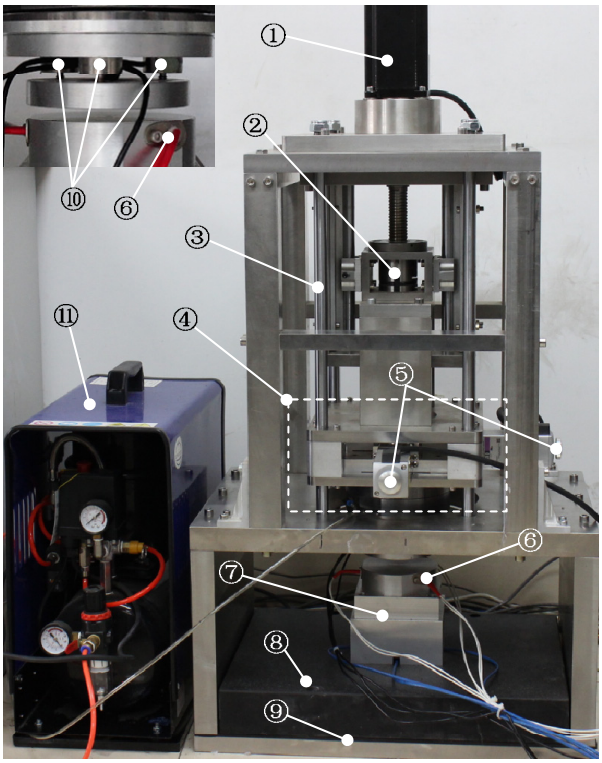

Fig. 6. NIL machine: ① z-axis actuator, ② preload ball screw, ③ precision cylinder, ④ parallel alignment stage, ⑤ x- or y-actuator, ⑥ cartridge heater, ⑦ substrate stage, ⑧ marble base, ⑨ rubber cushion, ⑩ force sensor, and ⑪ air compressor

It is known that the minimum feature size on the substrate is mainly determined by that on the template that can be fabricated. Further, considering the final manufacturing cost, a series of 2.5 μm wide grating patterns with a 3.5 μm period are fabricated on the silicon template using the electron-beam process. Polymethyl methacrylate (PMMA) is used as the substrate material due to its small thermal expansion coefficient of about 6.0×10^{-5} per °C and glass transition temperature (T_g) of about 105 °C. After accomplishing the imprint process, in order to carefully examine the grating patterns on the PMMA substrate using the scanning electron microscope (SEM), a thin Au film with thickness of a few nanometers is first uniformly deposited onto its entire surface. Fig. 7 shows the final SEM image of the grating patterns on the substrate surface, where the substrate temperature and imprinting force used in this experiment are about 145 °C and 1200 N, respectively. It can be seen that the grating patterns on the substrate are very uniform in a large area. But the 3.269 μm width and 2.534 μm period of the grating patterns are a little smaller than the corresponding values of the template, which is mainly attributed to the PMMA shrinkage resulting from the temperature drop during the demolding process. However, this shrinkage can be relieved

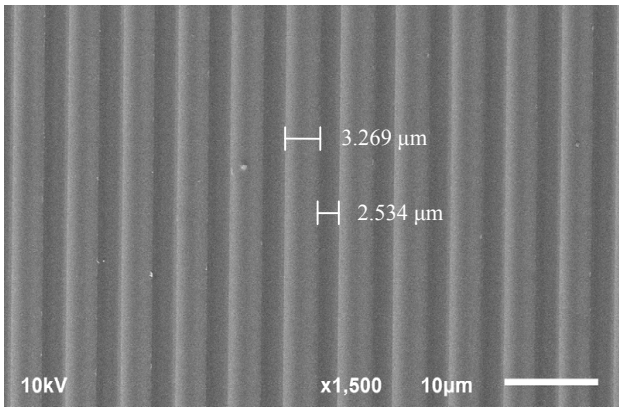

Fig. 7. SEM image of the grating patterns on the substrate surface

by the temperature control. This imprint result still demonstrates that the proposed alignment stage can be used in the hot embossing process. In the next research, we will conduct the nano-level pattern transfer between the template and the substrate to verify the deep performance of the proposed alignment stage.

VI. Conclusion and Future Work

This paper presents the development of a force-decoupled compound parallel alignment stage to guarantee the alignment accuracy especially under a large imprinting force for the hot embossing NIL. It consists of a high-stiffness SAB and a delicate multi-DOF flexure-based mechanism. The template center coincides with the spherical center of the SAB stator or rotor to avoid the coupled lateral motion of the template due to its tilt. The large imprinting force is supported by the high-stiffness SAB, whereas only the small bending moment due to the nonuniform imprinting force can reach the flexure-based mechanism. The alignment capacity of the parallel alignment stage is mainly determined by the stiffness of the multi-DOF flexure-based mechanism along the different motion directions. Finite element analysis has been utilized to investigate the performance of the parallel alignment stage and examine the accuracy of the established models. The NIL machine is constructed and tested for the hot embossing process. The 2.5 μm wide grating patterns with a 3.5 μm period are successfully transferred from the silicon template to the PMMA substrate. The substrate temperature and imprinting force used in this experiment are about 145 °C and 1200 N, respectively.

The addressed parallel alignment problem in this paper is mainly aimed at the hard plate-to-plate based NIL, and does not exist on the gas press and soft-template based NIL. But all of them are only restricted to the small-size template due to their own disadvantages. In contrast, the roll-to-roll NIL can achieve a large-size imprint with high efficiency. However, the resolution of the latter is more lower that that of the former. In the further research, we hope that the proposed force-decoupled concept can be extended to the structure design of the roll-to-roll NIL to further improve its resolution.

References

[1] S. Y. Chou, P. R. Krauss, and P. J. Renstrom, "Nanoimprint lithography", Journal of Vacuum Science and Technology B, vol. 14, pp. 4129-4133, 1996.
[2] S. Y. Chou and P. R. Krauss, "Imprint lithography with sub-10 nm feature size and high throughput", Microelectronic Engineering, vol. 35, pp. 237-240, 1997.
[3] D. Nilsson, T. Nielsen, and A. Kristensen, "Solid state microcavity dye lasers fabricated by nanoimprint lithography", Review of Scientific instruments, vol. 75, pp. 4481-4486, 2004.
[4] H. Becker and U. Heim, "Hot embossing as a method for the fabrication of polymer high aspect ratio structures", Sensors and actuators A: Physical, vol. 83, pp. 130-135, 2000.
[5] S. Grego, A. Huffman, M. Lueck, B. R. Stoner, and J. Lannon, "Nanoimprint lithography fabrication of waveguide-integrated optical gratings with inexpensive stamps", Microelectronic Engineering, vol. 85, pp. 1846-1851, 2010.
[6] Y. Wang, S. H. Goh, X. Bi, and K. L. Yang, "Replication of DNA submicron patterns by combining nanoimprint lithography and contact priniting", Journal of Colloid and Interface Science, vol. 333, pp. 188-194, 2009.
[7] W. Zhang and S. Y. Chou, "Multilevel nanoimprint lithography with submicron alignment over 4 in. Si wafers", Applied Physics Letters, vol. 79, pp. 845-847, 2001.
[8] H. Lan, Y. Ding, H. Liu, and B. Lu, "Review of the wafer stage for nanoimprint lithography", Microelectronic Engineering, vol. 84, pp. 684-688, 2007.
[9] L. J. Guo, "Nanoimprint lithography: methods and material requirements", Advanced Materials, vol. 19, pp. 495-513, 2007.
[10] L. L. Howell, Compliant Mechanism, New York: Wiley, 2001.
[11] X. Sun, W. Chen, Y. Tian, S. Fatikow, R. Zhou, J. Zhang, and M. Mikczinski, "A novel flexure-based microgripper with double amplification mechanisms for micro/nano manipulation", Review of Scientific Instruments, vol. 84, pp. 085002-1-085002-10, 2013.
[12] Y. Tian, B. Shirinzadeh, and D. Zhang, "Design and dynamics of a 3-DOF flexure-based parallel mechanism for micor/nano manipulation", Microelectronic Engineering, vol. 87, pp. 230-141, 2010.
[13] D. Zhang, D. G. Chetwynd, X. Liu, and Y. Tian, "Investigation of a 3-DOF micro-positioning table for surface griding", Internation Journal of Mechanical Sciences. vol. 48, pp. 1401-1408, 2006.
[14] D. Kang and D. Gweon, "Development of flexure based 6-degrees of freedom parallel nano-positioning system with large displacement", Review of Scientific Instruments, vol. 83, pp. 035003-1-035003-9, 2012.
[15] K .B. Choi and J. J. Lee, "Passive compliant wafer stage for single-step nano-imprint lithography", Review of Scientific Instruments, vol. 76, pp. 075106, 2005.
[16] J. J. Lee, K. B. Choi, and G. H. Kim, "Design and analysis of the single-step nanoimprinting lithography equipment for sub-100 nm linewidth", Current Applied Physics, Vol. 6, pp. 1007-1011, 2005.
[17] X. Jia, J. Liu, Y. Tian, and D. Zhang, "Stiffness analysis of a compliant precision positioning stage", Robotica, vol. 30, pp. 925-939, 2012.
[18] B. J. Choi, S. V. Sreenivasan, S. Johnson, M. Colburn, and C. G. Wilson, "Design of orientation stages for step and flash imprint lithography", Precision Engineering, vol. 25, pp. 192-199, 2001.
[19] C. Du, W. Chen, Y. Wu, W. Chen, and M. Yuan, "Development of a force-decoupled parallel alignment device for nanoimprint applications", Proceedings of the Institution of Mechanical Engineers, Part B: Journal of Engineering Manufacture, vol. 228, pp. 127-139, 2014.
[20] X. Sun, W. Chen, R. Zhou, J. Zhang, and W. Chen, "Development of a flexure-based XY positioning stage for micro/nano manipulation", Proceedings of the Third International Conference on Manipulation, Manufacturing and Measurement on the Nanoscale, Suzhou, China, 2013.
[21] X. Sun, W. Chen, R. Zhou, W. Chen, and J. Zhang, "A decoupled 2-DOF flexure-based micropositioning stage with large travel ranges", Robotica, pp. 1-18, 2013.
[22] W. C. Young and R. G. Budynas, "Roarks Formulas for Stress and Strain", New York: McGraw-Hill, 2002.
[23] H. H. Pham and I. M. Chen, "Stiffness modeling of flexure parallel mechanism", Precision Engineering, vol. 29, pp. 467-478, 2005.
[24] Y. Li and Q. Xu, "Design and analysis of a totally decoupled flexure-based XY parallel micromanipulator", IEEE Transactions on Robotics, vol. 25. pp. 545-657, 2009.